



Processing of titanium alloys with improved efficiency and accuracy by laser and electrochemical machining

Yong Yang^{1,2,3} · Yufeng Wang^{1,2,3} · Chenyu Sun^{1,4} · Qiang Wu⁴ · Jie Yan⁴ · Yunfeng Liu⁵ · Jianhua Yao⁵ · Wenwu Zhang^{1,2,3}

Received: 28 September 2023 / Accepted: 3 January 2024 / Published online: 11 January 2024
© The Author(s), under exclusive licence to Springer-Verlag London Ltd., part of Springer Nature 2024

Abstract

The fabrication of microstructures with high efficiency and accuracy on titanium alloys presents significant challenges due to stringent quality requirements. Hybrid laser and electrochemical machining (LECM) has emerged as a viable solution for efficient and precise processing of titanium alloys. This study investigates the material removal mechanism of titanium alloys during LECM, analyzing the machining characteristics under the combined influence of laser processing and electrochemical machining. The impacts of voltage, laser power, and feeding rate on aspects such as aspect ratio, accuracy, efficiency, and surface roughness are examined. Results reveal that synchronous laser irradiation effectively accelerates electrochemical corrosion rates, enhancing the removal capability of the passive film. Notably, LECM outperforms pure ECM, demonstrating significant improvements in parameters such as aspect ratio (394.4% increase), material removal rate (140% increase), and side gap (172.8% increase). Lower laser power is favored for high-precision LECM. An electric circuit model elucidates the titanium alloy material removal mechanism in LECM. Additionally, the study proposes the use of gradient laser power for fabricating high-aspect-ratio structures with efficiency and accuracy. The research successfully fabricates microstructures with elevated aspect ratio and flat bottoms on titanium alloys.

Keywords Titanium alloy · Laser and electrochemical machining · Aspect ratio · Machining accuracy · Materials removal rate

1 Introduction

Titanium alloys possess unique characteristics, including low density, excellent mechanical properties, high corrosion resistance, and elevated working temperature. These

attributes make titanium alloys valuable for applications in aerospace, biomedical, and other industries [1]. The quality of processing is intricately linked to the performance and longevity of components made from titanium alloy. However, due to its high strength, low thermal conductivity, and substantial tensile strength, processing titanium alloy proves challenging. The machining of titanium remains problematic, as mechanical processes endure tool wear and surface defects like heat-affected zones, microcracks, and burrs. These factors, along with high costs and surface defects inherent to mechanical processing, hinder the widespread use of titanium alloy. Consequently, non-conventional machining processes are considered competitive alternatives for achieving high surface quality and cost-effectiveness in titanium alloy processing, such as laser beam machining (LBM), electric discharge machining (EDM), electrochemical machining (ECM), and hybrid machining processes. Numerous investigations have been conducted to explore the mechanism of titanium alloy machining.

✉ Yufeng Wang
wangyufeng@nimte.ac.cn

Yong Yang
1261842788@qq.com

¹ Chinese Academy of Sciences, Ningbo Institute of Materials Technology and Engineering, Ningbo 315201, China

² Key Laboratory of Aero Engine Extreme Manufacturing Technology of Zhejiang Province, Ningbo 315201, China

³ University of Chinese Academy of Sciences, Beijing 100049, China

⁴ Suzhou Electric machining Machine Tool Research Institute Co, Ltd., Suzhou 215011, China

⁵ College of Mechanical Engineering, Zhejiang University of Technology, Zhejiang 310023, Hangzhou, China

LBM has found wide application in titanium alloy processing, encompassing welding, cleaning, and additive manufacturing [2–4]. Previous studies predominantly employed LBM for creating surface micro-textures. For instance, He et al. utilized re-solidification bulges resulting from nanosecond laser irradiation to fabricate multi-scale microgroove textures on blood-contacting implants. These microgrooves had periods ranging from 15 to 35 μm and depths ranging from 20.5 to 25.6 μm [5]. Moura et al. identified resolidified material, debris, and microcracks in the microgroove [6]. Bloyce et al. discovered that the thermal oxidation of titanium could produce a thick, highly crystalline rutile oxide film [7]. Kumar et al. noted that laser processing could remove the surface oxide layer from titanium [8]. However, the cumulative heat effect induced by the low thermal conductivity of titanium alloy could lead to severe thermal damage.

EDM efficiently removes materials through high-temperature pulse sparks. Ayesta et al. employed EDM to create nozzle guide vanes with a depth of 6.5 mm [9]. Flaño et al. achieved stable machining of 25 mm depth grooves using proposed multi-holed electrodes, reducing process time by 65% for machining 10 mm depth grooves [10]. However, recast layers and thermal damage are inevitable in EDM. Pramanik et al. observed that EDMed surfaces consist of multi-layered recast layers with cracks and micropores. Lin et al. indicated that melted material might cause discharge localization, arcing, and short circuiting during EDM [11]. Moreover, as a thermo-electrical process, harmful substances are emitted during machining, which is detrimental to environment [12].

ECM offers unique advantages such as no tool electrode wear, absence of thermal damage, and good surface finish [13]. Zhao et al. created deep narrow grooves in titanium alloys using a hollow slice cathode during ECM [14]. Wang et al. investigated the impact of mask aspect ratio on microgroove profiles during through-mask ECM, processing a group of 30 semi-circular microgrooves with a 52.59 mm radius in cross-section on titanium alloys [15]. Zhang et al. crafted a complex groove of 1.32 mm width and 8.05 mm depth through single-pass milling with a tube electrode. However, the electrode's maximum feed rate was just 0.42 mm/min, and taper in the entry portion could not be avoided with an uninsulated electrode [16]. Additionally, the complex oxide and polyvalent state at the interface between titanium alloy and electrolyte increase the difficulty of ECM for titanium alloy [17]. Prior studies demonstrated that increasing the concentration of halide ions [18], or using nonaqueous electrolyte [19] could accelerate the ECM rate. Consequently, optimizing the electrolyte composition during electrochemical machining of titanium alloys is crucial, as the machining rate remains low, constraining ECM's application in titanium alloy processing. Currently, the hybrid

ECM process has been introduced for efficiently machining titanium alloys while retaining ECM's benefits. Nguyen et al. enhanced dimensional accuracy and surface integrity by simultaneously using electric discharge milling and electrochemical milling, indicating that the recast layer could be reduced at a low feeding rate of 10 $\mu\text{m/s}$ [20]. Zhai et al. integrated megasonic vibration into the through-mask ECM process to improve machining precision and deep etching capability, resulting in micro pits with an average depth-diameter ratio of 0.47 [21]. Li et al. examined the machining characteristics of ultrasonic-assisted electrochemical grinding of titanium alloys, detecting a titanium dioxide layer with a 78 nm thickness on the surface [22]. Laser has also been integrated into ECM, referred to as laser and electrochemical machining (LECM), to enhance the material removal rate (MRR) and machining precision. Wang et al. demonstrated that the MRR and machining precision could be augmented by 122.7% and 60.7%, respectively [23]. However, limited studies have explored the machining characteristics of titanium alloys during LECM, particularly microstructures with a higher aspect ratio.

This study employed the laser and shaped tube electrochemical machining (Laser-STEM) process to fabricate high-aspect-ratio microgrooves on titanium alloys. By controlling the hybrid tubular electrode's lateral movement, microstructures are produced through Laser-STEM. We investigated the mechanism of material removal in titanium alloys under the combined influence of laser processing and ECM. The study examined the machining characteristics of titanium alloys during Laser-STEM, considering various laser powers, voltages, and feeding rates of the tool electrode. Additionally, we proposed the use of gradient laser power to ensure accuracy and MRR in Laser-STEM of microgrooves on titanium alloys.

2 Materials and methods

2.1 Mechanism of laser and electrochemical machining

The mechanism of LECM is depicted in Fig. 1a. The outer layer of the hybrid tool electrode consists of an insulated metal tube. Within this tube, a hollow polytetrafluoroethylene (PTFE) capillary is positioned. The electrolyte flows through this capillary to reach the machining zone. Due to the lower refractivity of PTFE ($n_2 = 1.24$) compared to that of the electrolyte ($n_1 = 1.35$), the laser beam can be transmitted along the electrolyte flow through internal total reflection. This occurs at an incident angle greater than θ_c ($\arcsin(n_2/n_1)$), enabling the laser to act on the central machining zone (Fig. 1b). In the LCEM process, laser power density is concentrated mainly in the central machining area.

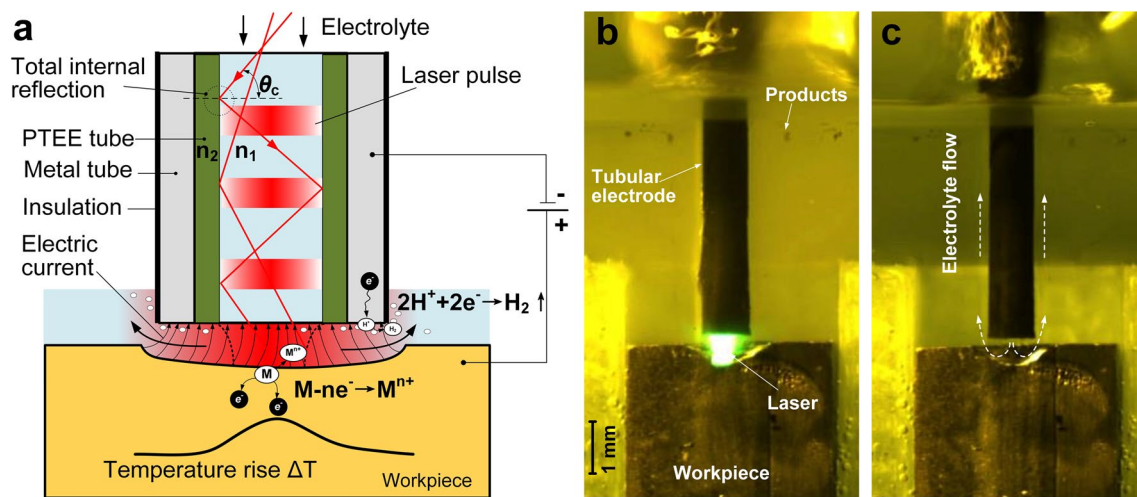


Fig. 1 Schematic diagram of the laser and electrochemical machining processes, **a** Schematic diagram of LECM, **b** Photograph of the machining process with laser acting on the machining zone, **c** Photograph of the machining process during laser off-time

Laser-induced temperature rise enhances local electrolyte conductivity, promoting electrochemical corrosion efficiency in this area. With higher laser power, laser processing can remove both the titanium alloys and the passivation layer. Simultaneously, ECM contributes to material removal, ensuring machining surface quality. Figure 1c illustrates that during laser pulse off-time, the electrolyte flowing from the inner hole of the tubular electrode flushes out electrolytic products, microbubbles, and sludges generated by laser processing. This continuous action of the laser in the machining zone enhances efficiency.

2.2 Experimental setup

An experimental setup was devised for LECM (Fig. 2). The electrolyte was filtered and pumped to the hybrid tubular electrode. A 532 nm green laser source was chosen to minimize attenuation during laser transmission in the electrolyte (attenuation coefficient: $4.5 \times 10^{-4} \text{ cm}^{-1}$) [24]. The laser beam was focused at the entrance of the hybrid tubular electrode and introduced into the electrolyte flow. A three-dimensional motion platform enabled control of the relative position between the tubular electrode and the workpiece. This platform had a travel range of 250 mm \times 250 mm \times 150 mm and a resolution of 0.1 μm . Pulse voltage source terminals were connected to the workpiece and the electrode. A digital oscilloscope monitored the electrochemical process, aiding electrode gap control.

2.3 Materials and measurement

Workpieces made of titanium alloy TC4 with a 3-mm thickness and a surface roughness of $R_a 1.6 \mu\text{m}$ underwent LECM processing. The electrode's metal tube was composed of

titanium, possessing an inner diameter of 0.8 mm and an outer diameter of 1.2 mm. The sidewall of the metal tube was coated with a 30- μm -thick electrical insulation material. A PTEE tube with an inner diameter of 0.5 mm and an outer diameter of 0.73 mm was inserted within the metal capillary. Other experimental conditions are detailed in Table 1.

Before and after processing, workpieces were cleaned in absolute alcohol using an ultrasonic washer for 15 min. A laser scanning microscope (Keyence, VK-X200K) measured the three-dimensional (3D) geometrical dimensions of the processed grooves. Scanning electron microscopy (SEM, SU5000, Hitachi) revealed the microscopic features of the machining area and element distribution. Experiments with varying parameters were repeated three times, and the results were averaged. Aspect ratio and MRR indicated processing capacity. The measurement criteria are illustrated in Fig. 3. The machining side gap represented processing accuracy, calculated as the average difference between the hybrid tool electrode's outer diameter and the processed groove width. Surface roughness R_a of the groove bottom assessed processing quality.

3 Machining characteristics of titanium alloys by LECM

3.1 LECM of titanium alloys with the smaller voltage: influences of voltage

Figure 4a depicts the changes in aspect ratio and machining side gap of the LECM-processed grooves in response to varying voltages. The feeding rate stood at 1.80 mm/min, and the initial electrode gap was 0.30 mm. A laser power of 3 W was employed. Notably, the side gap and aspect ratio

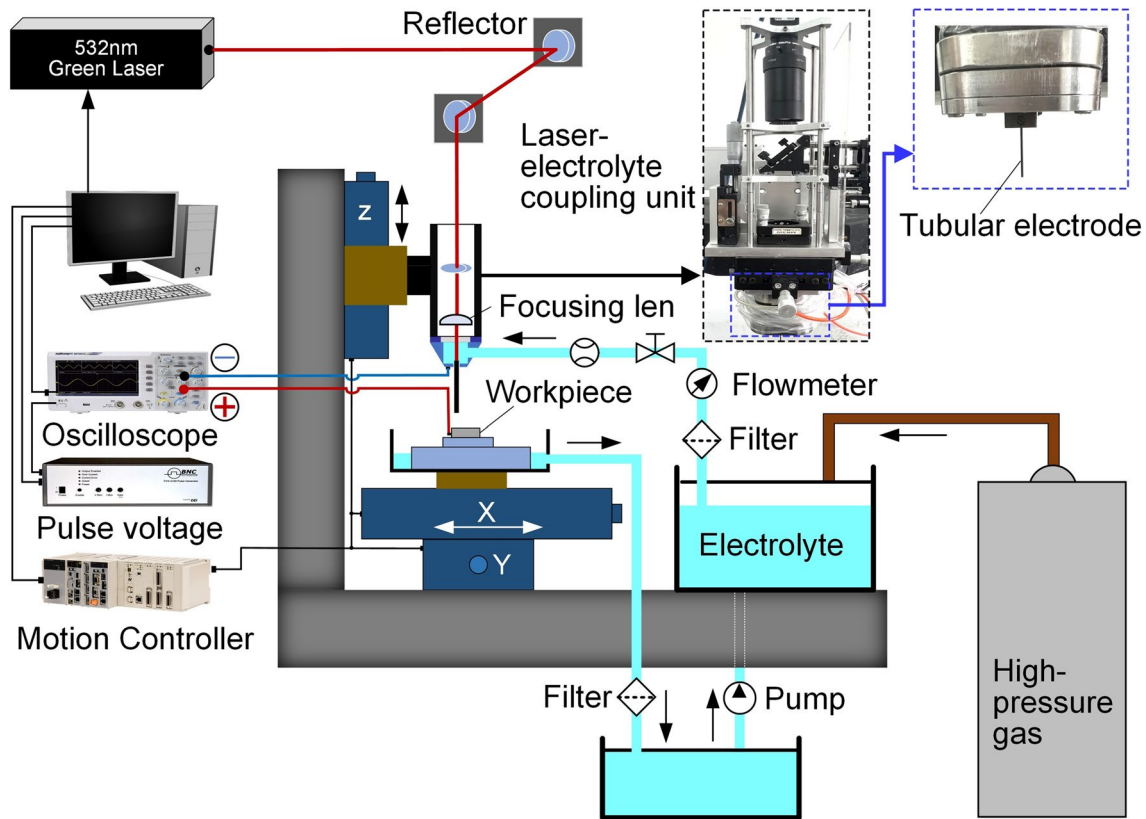


Fig. 2 Schematic diagram of the experimental setup developed for LECM

Table 1 Experimental conditions for LECM

Parameter	Unit	Value
Voltage (U_w)	V	12–24
Pulse frequency	kHz	20
Duty cycle	%	50
Electrolyte concentration	g/L	12.5% NaNO_3
Electrolyte pressure	MPa	0.3
Electrolyte flow rate	mL/min	100
Laser power	W	0–9
Laser pulse width	ns	16
Repetition frequency	kHz	8
Temperature	$^{\circ}\text{C}$	24

experienced increases of 172.8% and 77.9%, respectively, as the voltage rose from 12 to 24 V.

Figure 4b illustrates the alteration in Material Removal Rate (MRR) with laser power levels of 3 W and 0 W. The MRR of single ECM without laser was notably lower than that of LECM, particularly within the voltage range of 12 to 18 V. Below 18 V, single ECM struggled to remove titanium alloy material effectively. The laser-induced temperature-rise boosted ion transport efficiency and electrolyte conductivity, thus enhancing ECM rate. However, as the

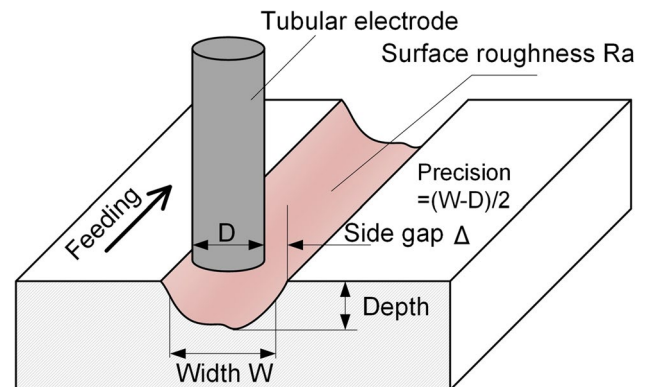
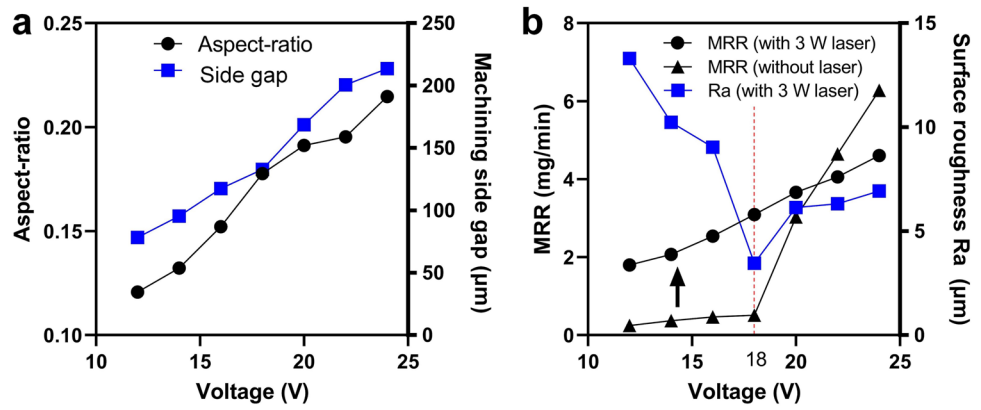


Fig. 3 Schematic diagram for the measurement of the microgroove processed by LECM

voltage escalated from 18 to 24 V, the MRR of single ECM surged from 0.51 to 6.28 mg/min, surpassing even the MRR achieved by 3 W power LAECM for voltages exceeding 21 V. This unexpected increase may be attributed to decreased machining accuracy without laser utilization. The rise of side gap would increase the MRR more efficiently than the aspect ratio. At higher voltages, the electric current density distribution in single ECM process extended toward the periphery, potentially leading to stray corrosion.

Fig. 4 **a** Variations in the aspect ratio and side gap of the microgrooves processed by LECM with voltage, **b** Variations in the MRR and surface roughness Ra with voltage



Surface roughness Ra, resulting from LECM, initially decreased as the voltage increased from 12 to 18 V. The rapid removal of a substantial oxide layer and processing of surface electrochemical solution morphology could be attributed to the elevated electric current density with increasing voltage. However, as the voltage increased from 18 to 24 V, roughness Ra rose from 3.46 to 6.13 μm. The surge in roughness was due to localized disruption of the oxide layer under high current density at voltages exceeding 18 V, resulting in localized peeling and deteriorated surface roughness. It was established that, with a voltage smaller than 22 V, LECM achieved higher MRR than pure ECM. However, when voltage surpassed 22 V, ECM’s MRR surpassed that of LECM due to increased

stray current-induced material removal. Thus, a voltage smaller than 22 V was recommended for LECM.

Figure 5 presents the cross-sectional profiles of processed microgrooves with voltages of 12 V and 18 V, alongside laser powers of 0 W and 4 W, respectively. At a voltage of 12 V, single ECM struggled to remove titanium alloys effectively, leading to the observation of micro pits. As the voltage increased to 18 V, a microgroove with a width of 1318.18 μm and depth of 48.05 μm could be processed. This was due to the high electric current density-induced breakdown of the oxide layer, resulting in electrochemical dissolving of titanium alloy material. Moreover, when the laser power increased to 4 W, microgroove depth increased, particularly in the central machining area. This indicated the efficiency-enhancing effect of temperature rise. With the

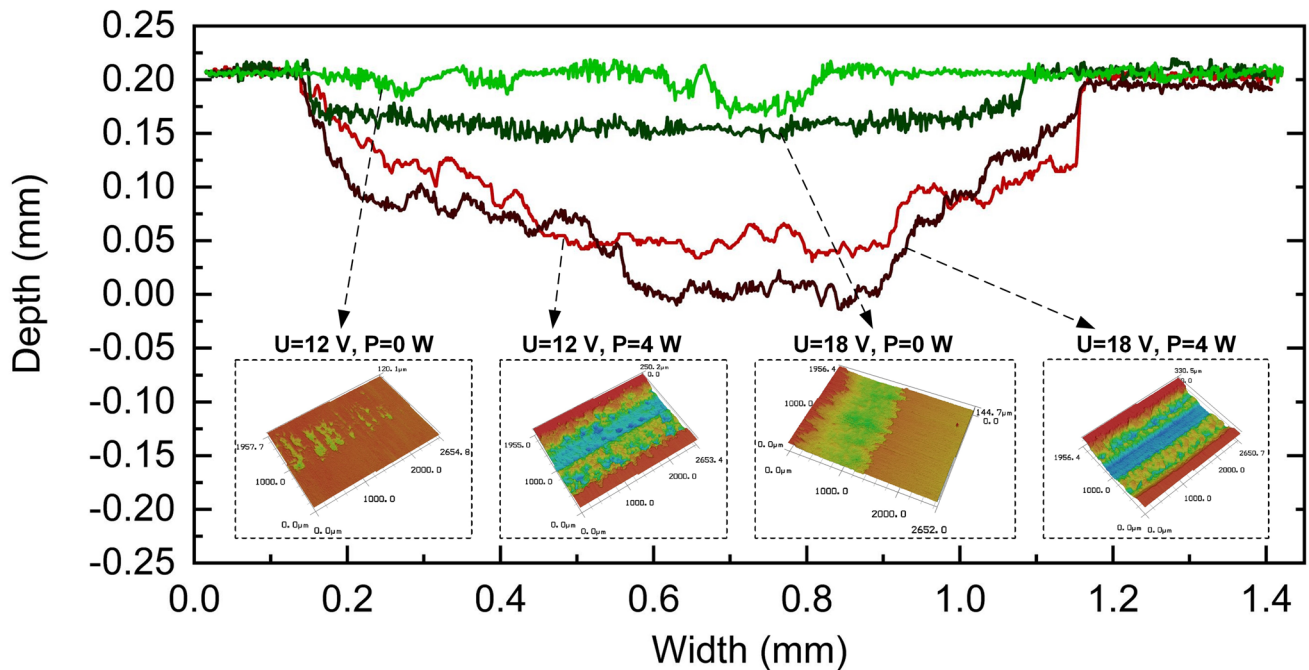


Fig. 5 Comparison of the cross-sectional profile of the processed microgrooves under different conditions through LECM and ECM process

voltage at 18 V, a microgroove with a width of 1465.55 μm and a depth of 260.33 μm could be processed. Compared to the geometry of microgrooves processed by a single ECM at 18 V, width, depth, and aspect ratio increased by 11.18%, 441.79%, and 394.44%, respectively.

3.2 Improving ECM accuracy and efficiency by laser: influences of laser power

Figure 6a illustrates the changes in aspect ratio and machining side gap of microgrooves processed by LECM with laser power ranging from 0 to 5 W. The voltage was set at 18 V, and the feeding rate was 1.8 mm/min. Aspect ratio of processed microgrooves increased by 157.3% as laser power reached 5 W. This enhancement primarily affected depth rather than width, attributable to the accelerated passive film removal rate in ECM due to the temperature-rise effect induced by laser irradiation. Machining side gap was reduced by 33.6% with laser power increased to 3 W. The laser-heated local electrolyte, flowing from the central area, expedited oxide film formation. The thickened film hindered active anion traversal to the metal-oxide layer interface, impeding electrochemical reaction. Simultaneously, central laser irradiation promoted oxide layer removal in ECM and concentrated electric current in the central processing area, thereby improving accuracy. However, as laser power rose from 3 to 5 W, side gap increased from 147.68 to 194.28 μm . Reduced machining accuracy could be attributed to excessive temperature rise in the peripheral region and concentrated electric current in the peripheral area, caused by direct removal of central material using high laser power.

As depicted in Fig. 6b, the Material Removal Rate (MRR) of LECM experienced a 140% increase, rising from 1.95 to 4.68 mg/min, with laser power ranging from 0 to 5 W. This enhancement resulted from the acceleration of the ECM rate due to elevated electrolyte temperature. Additionally, the laser processing directly removed titanium alloys. Simultaneously, the surface roughness value R_a diminished from 7.65 to 5.1 μm as laser power increased from 0 to 3 W. This

improvement can be attributed to the enhanced capability and homogeneity of electrochemical dissolution within the machining area with increased laser power. During milling, peripheral material primarily experienced erosion via single ECM with laser-heated electrolyte, while central material removal occurred through LAECM with direct laser beam irradiation. Consequently, the electrolyte's heating effect led to uneven dissolution of substrate material, negatively affecting surface roughness. However, increasing laser power to 3 W reduced the difference in processing capability distribution, leading to a decrease in surface roughness R_a to 5.1 μm . Subsequently, elevating the laser power from 3 to 5 W resulted in an increase in surface roughness R_a to 8.28 μm , surpassing that of microgrooves processed by single ECM. This unexpected surface roughness increase can be attributed to direct removal of titanium alloy material once laser power density exceeded the ablation threshold, possibly creating a slot along the center line. Moreover, the laser power-induced temperature rise effect would accelerate surrounding ECM rates, intensifying stray corrosion and deteriorating surface finish.

Figure 7 displays the cross-sectional profiles of microgrooves processed with different laser power levels. Employing a voltage of 18 V and a feeding rate of 1.8 mm/min, a flat bottom was achieved at a laser power of 3 W. Raising the laser power to 6 W resulted in the formation of a micro slot with a conical angle at the bottom, attributed to the influence of high-power-density laser beam. However, when compared to the profile at 3 W, the edge morphology remained largely consistent. Nevertheless, the bottom's surface became more undulating with a laser power increase to 6 W, potentially attributed to the inhomogeneous distribution of current density and electrolyte flow field due to laser processing products. At an applied laser power of 9 W, a high-aspect-ratio slot, with a depth exceeding 0.7 mm, was engraved in the central machining area. The profile indicated that materials surrounding were barely removed by the ECM process, suggesting that LBM dominated. This inhibition of surrounding ECM capability can be attributed to electrode-workpiece

Fig. 6 a Variation of the aspect ratio and side gap with laser power, b Variation of MRR and surface roughness R_a of the LECM-processed microgrooves with laser power

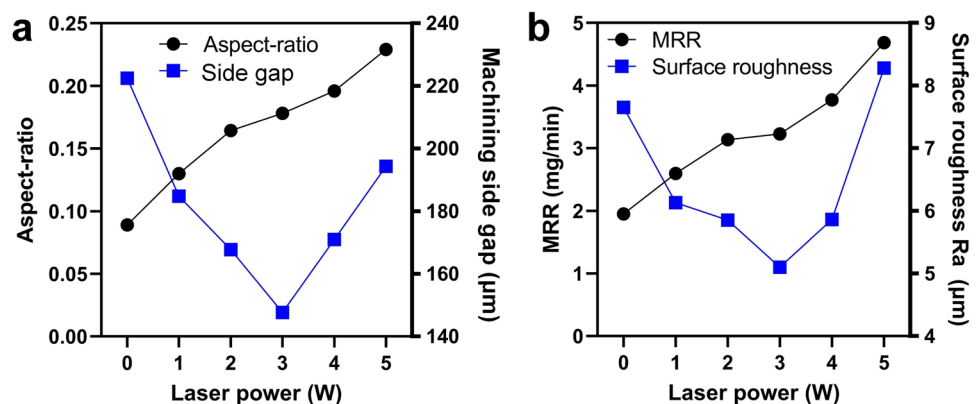
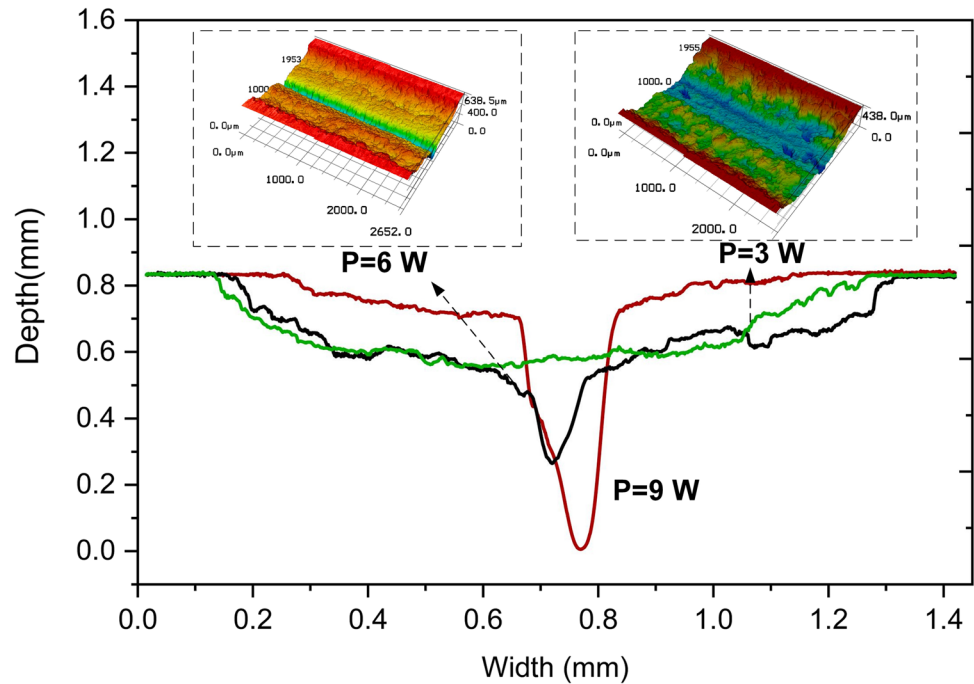


Fig. 7 Comparison of the cross-sectional profile of microgrooves processed by LECM with laser power of 3 W, 6 W, and 9 W



disconnection; the side wall of the slot processed with a laser power of 9 W guided reflected electrolyte flow into the air at high speed, not participating in the machining process.

The SEM images of the groove processed by LECM with a laser power of 9 W are shown in Fig. 8. Several spherical particles could be observed adhered to the wall, and the lump of molten metal could be seen at the bottom. Besides this, the image shows a typical electrochemical processed porous microstructure on the edge of the slot, indicating that the slot was processed by electrolyte jet assisted laser processing.

3.3 Effect of tubular electrode feeding rate

Figure 9a displays the alteration in aspect ratio and side gap of LECM-processed grooves as the feeding rate varied from 0.8 to 2.2 mm/min. A laser power of 3 W and voltage of 18 V were employed. Notably, the aspect ratio of processed

microgrooves decreased by 56.18%, with a feeding rate increase to 2.2 mm/min. This reduction corresponds to the decrease in processing time per unit length as the feeding rate increases. Similarly, the side gap decreased by 119.2% as the feeding rate increased from 0.8 to 2.2 mm/min. This reduction is attributed to diminished material erosion in the outer machining zone with higher feeding rates, resulting in decreased side gap. Hence, a higher feeding rate of the tubular electrode could enhance machining precision.

The decline in aspect ratio and side gap, alongside increased feeding rate, led to a decrease in MRR, as depicted in Fig. 9b. MRR can be represented as the product of feed length per unit time and sectional area. Surface roughness R_a decreased to $4.57 \mu\text{m}$ as the feeding rate increased to 1.8 mm/min, followed by an increase to $6.37 \mu\text{m}$ with a feeding rate of 2.2 mm/min. A low feeding rate can induce significant stray corrosion, negatively impacting surface finish. Laser-induced temperature rise can enhance ECM

Fig. 8 SEM image of the processed microgroove with a laser power of 9 W

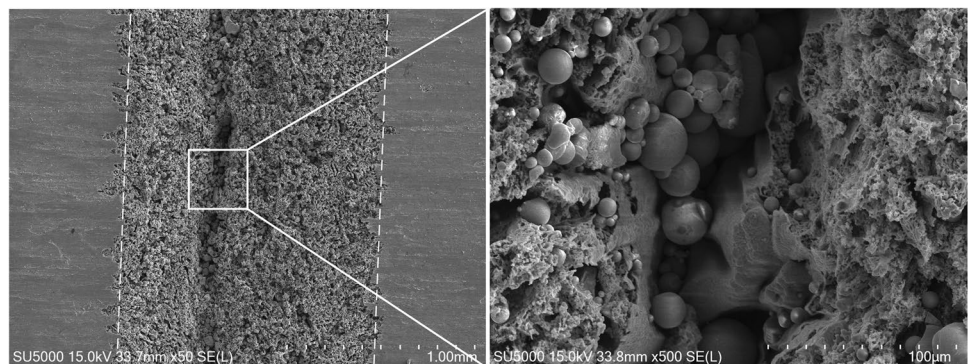
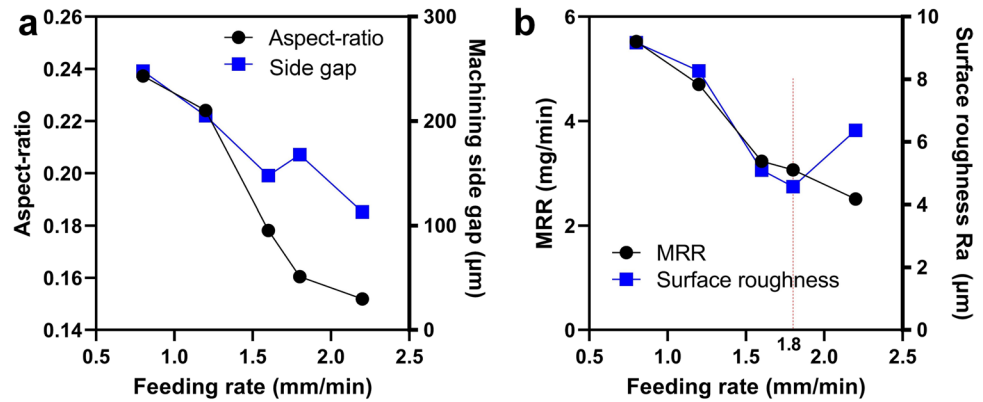


Fig. 9 **a** Variation of the aspect ratio and side gap of micro-grooves with feeding rate, **b** Variation of MRR and surface roughness Ra of LECM-processed grooves with feeding rate



removal capability on titanium oxide, while oxide formation can also be accelerated due to elevated electrolyte temperature. However, beyond a feeding rate of 1.8 mm/min, the materials removal reaction and oxide formation might not proceed optimally, resulting in surface roughness increase and lamellar exfoliation structure formation. Furthermore, excessive feeding rate could lead to insufficient materials removal, further deteriorating surface finish.

3.4 LECM with gradient laser power: strategies for high-precision processing

Experimental findings highlight that higher laser power can improve machining precision, aspect ratio, and materials removal rate. However, using high laser power could lead to micro slot processing at the central machining area due to the direct laser removal of titanium alloys. To enhance the accuracy of the bottom of microgrooves processed through LECM, a strategy involving gradient laser power has been proposed. In this approach, higher laser power is initially used to improve machining efficiency, followed by lower laser power to enhance machining accuracy, as depicted in Fig. 10a. This process entails utilizing higher laser power in LECM for efficient material removal, creating a deep, narrow groove with a microcavity at the center. Subsequently, lower laser power in LECM is employed to remove the central microcavity and enhance the surface finish of microgrooves.

Figure 10b presents three-dimensional and cross-sectional profiles of a reciprocating ling shape microgroove processed with a laser power of 5 W during LECM. A central microcavity was observed in the bottom of the cross-sectional profiles. Figure 10c displays an annular groove processed with a laser power of 5 W during LECM, revealing a conspicuous deep slot ablated by laser in the central area. Subsequently, when a laser power of 3 W was employed following 5 W power in LECM, as shown in Fig. 10d, the annular groove achieved a flat bottom. The initial machining electrode gap was set to 100 μm , and the feeding depth after first scanning

was of 400 μm . Thus, the LECM process with gradient laser power balances processing efficiency and accuracy, particularly for high-aspect-ratio microgroove fabrication.

Figure 11 displays the cross-sectional profiles of microgrooves employing gradient laser power. Achieving a flat bottom with surface roughness Ra of 3.3 μm demonstrates that using high-power laser first followed by low-power laser does not affect the surface finish of processed grooves. Moreover, the average processing depth within one sweep at a laser power of 5 W exceeded 415 μm , which was 1.5 times that achieved using 3 W laser power.

4 Discussion

The incorporation of laser into the Electrochemical Machining (ECM) process for titanium alloys enhances both precision and materials removal rate. To elucidate the mechanisms of titanium alloy material removal, an electric circuit model has been formulated, illustrated in Fig. 12. Herein, electrolyte resistance is denoted as $R_e(T)$, passivation layer resistance as R_o , and double layer resistance as R_{DL} . In the LECM process, laser beam transmission along the electrolyte flow is confined by total internal reflection within the PTEE capillary. This results in a laser power density distribution primarily concentrated in the central processing area, following a Gaussian distribution. Experimental findings indicate that single ECM struggles to remove titanium alloy materials under low voltage, i.e., below 18 V, due to the intact passivation layer under low electric field intensity. A passivation layer forms on titanium alloy surfaces, hindering electric current flow across resistance R_o . During LECM, laser irradiation at the central machining zone removes the passivation layer and elevates local electrolyte temperature, thereby lowering electrolyte resistance. Consequently, the total resistance of the equivalent electric circuit at the central machining zone is minimized. This high electric current density results in the greatest depth at the central machining zone. The Gaussian distribution of laser intensity across the

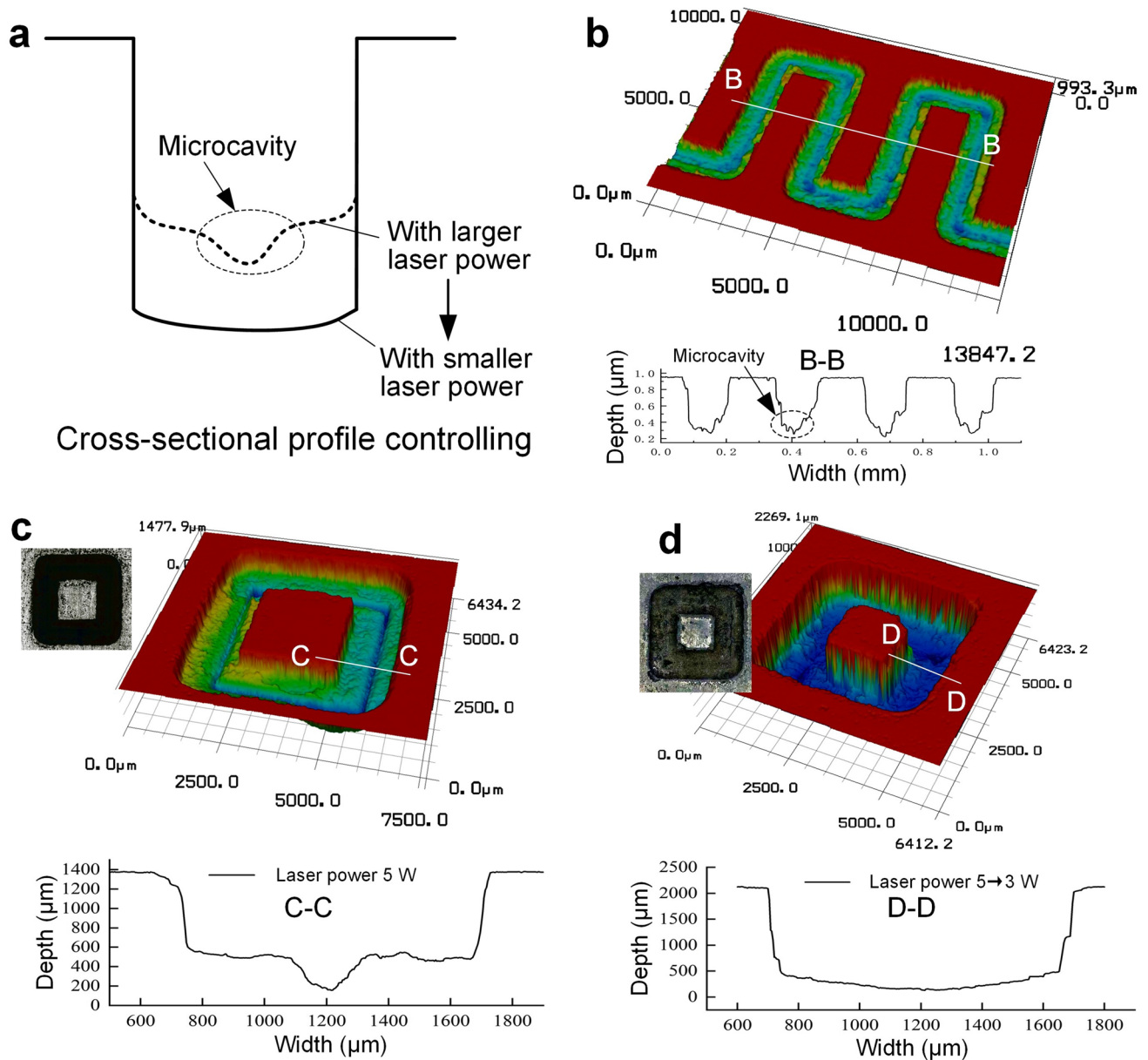
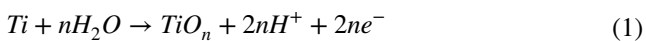


Fig. 10 **a** Schematic illustration of LECM using gradient laser power, **b** Three-dimensional and cross-sectional profiles of reciprocating ling shape microgroove processed with laser power of 5 W during LECM,

c Annular microgroove processed with laser power of 5 W during LECM, and **d** Annular groove processed by LECM with gradient laser power of 5 W first and then 3 W

machining area leads to a consistent depth reduction with radius increase, aligning with experimental observations.

Furthermore, laser-induced temperature rise at the surrounding machining area enhances passivation layer formation, expressed by the reaction (1):



This leads to increased passivation layer resistance R_o in the surrounding machining area. The enhanced passivation layer reduces stray corrosion effects, enhancing ECM

machining precision. Simultaneous laser irradiation on the machining zone contributes to this improvement. As electric current is primarily constricted beneath the tubular electrode, the aspect ratio of microgrooves on titanium alloys can be raised by increasing laser power during LECM.

A laser beam profiler (SP920s-1550, Ophir-Spiricon) visualized the Gaussian distribution of laser power density on the machining area, as depicted in Fig. 13a. The power of laser source was set to 0.4 W, and a series of attenuators was positioned in the laser transmission path before coupling. This confirms the confinement of the laser beam

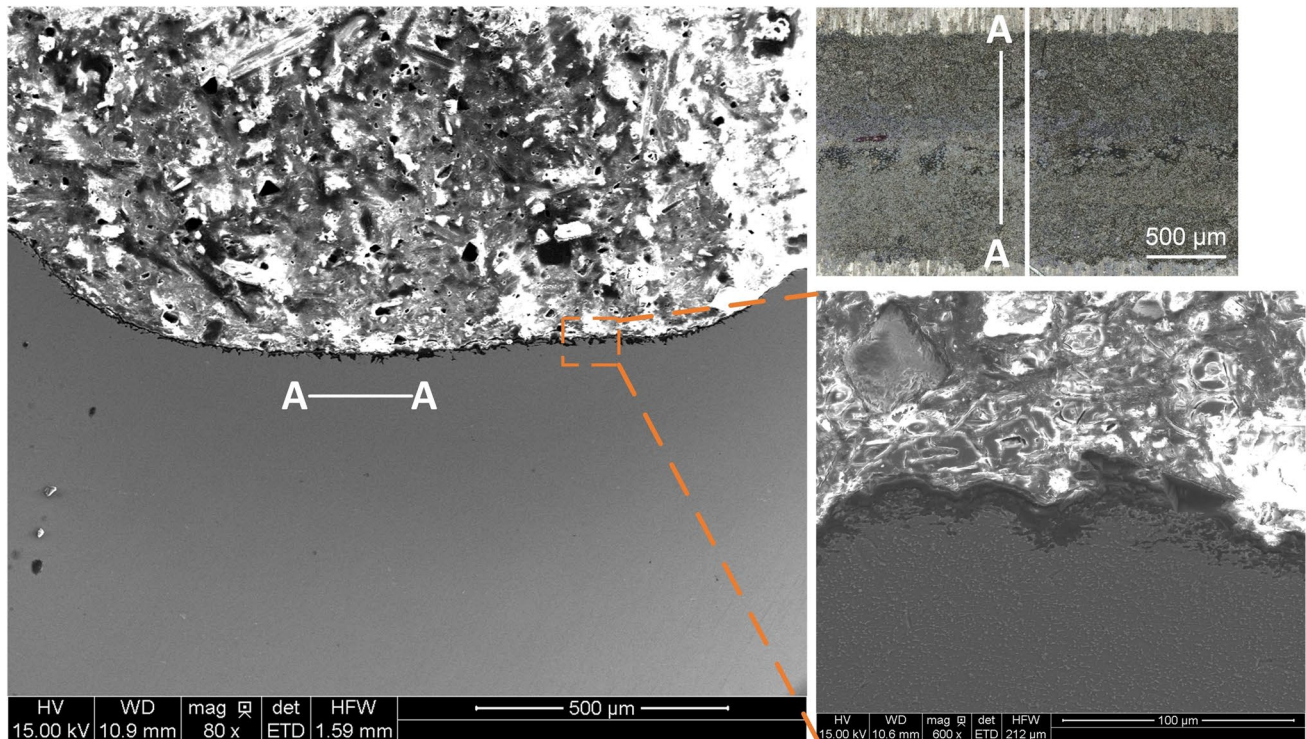


Fig. 11 The cross-sectional profiles of processed microgrooves using gradient laser power during LECM

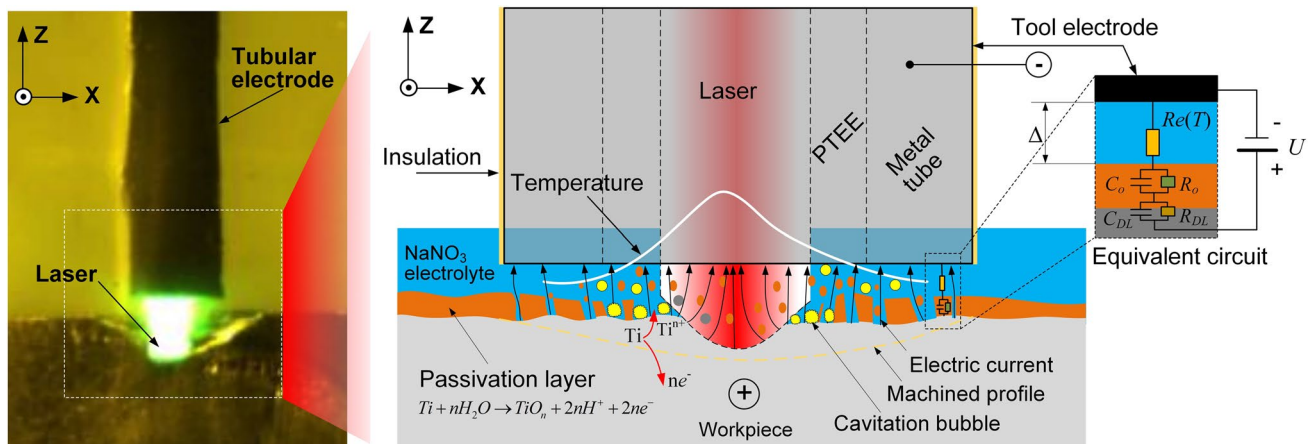


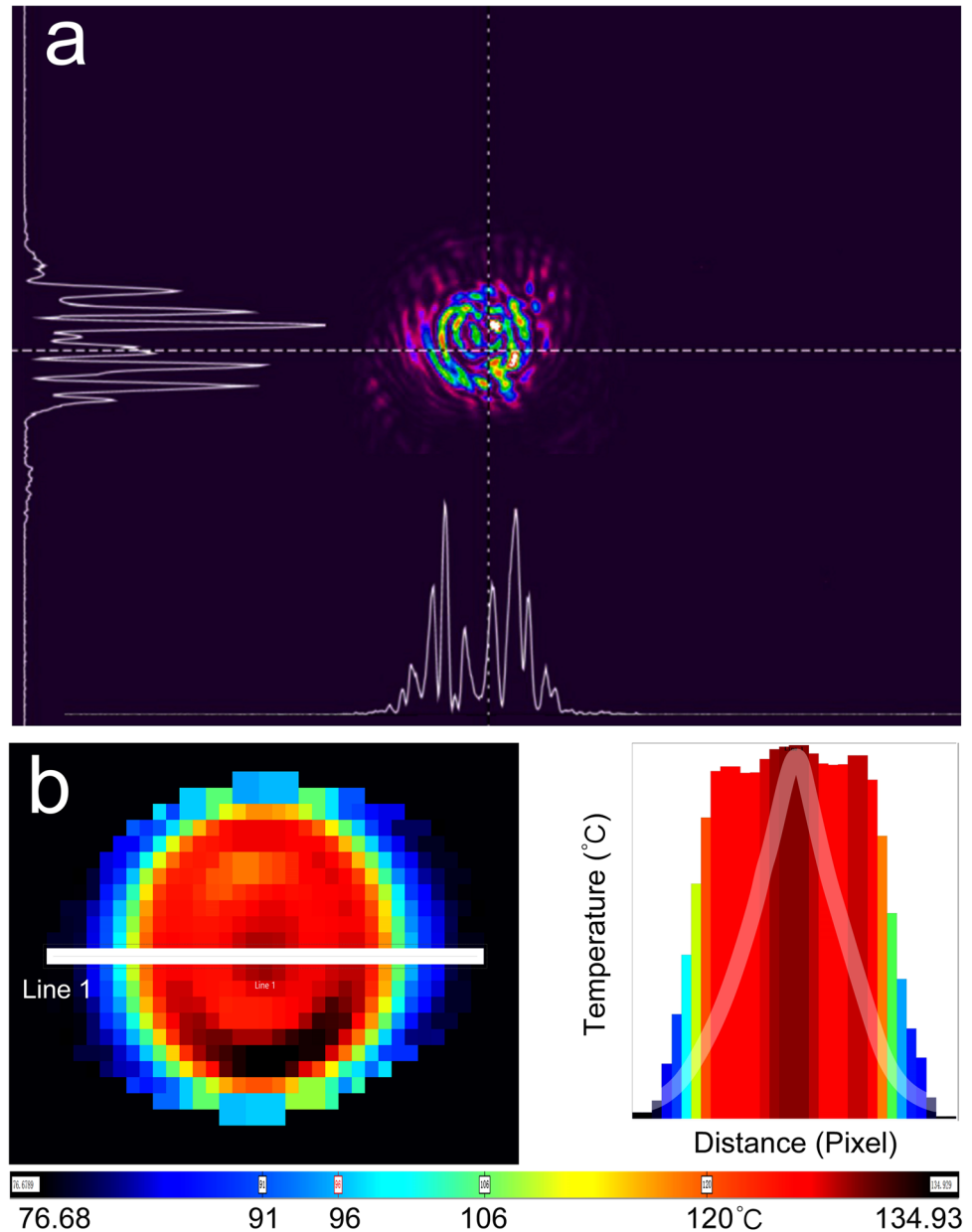
Fig. 12 Schematic illustration of the mechanisms for titanium alloy removal and equivalent electric circuit model of the LECM process

within the inner hole of the tubular electrode. Temperature distribution across the machining area was measured using a thermal infrared imager (TELOPS), displayed in Fig. 13b. The average export laser power was set to 5 W. The highest temperature was recorded at the central machining zone, with the surrounding machining area temperature around 76.68 °C. This temperature distribution

aligns with the microgroove profiles on titanium alloys processed through LECM, as discussed above.

The morphology of titanium alloys processed by LECM was observed through SEM. Figure 14 presents the oxygen content distribution on the machined surface. EDX results reveal a higher oxygen fraction at the edge of the processed structure, attributed to titanium oxide formation. Laser-induced temperature elevation of local electrolyte accelerates

Fig. 13 **a** Distribution of laser power density at the hybrid tool electrode outlet, and **b** Temperature distribution across the machining area



oxidation layer formation on titanium alloy surfaces. The transition region SEM image displays a corrosion stripping structure of the dense oxide layer. Laser processing can remove the oxide layer from the central machining area. SEM image within the central processing area presents a typical porous structure of electrochemical corrosion on titanium, with an exposed metal matrix at the bottom. The synergy between laser irradiation and electrochemical dissolution can breach the passive film restriction at the central machining area. Additionally, laser-induced temperature elevation enhances oxide layer

growth at the processed structure's edge, bolstering titanium alloy processing accuracy in the LECM process.

5 Conclusions

This study has employed LECM for microgroove and 3D microstructure fabrication on titanium alloys. The research has both theoretically and experimentally explored materials removal mechanisms, as well as the influences of

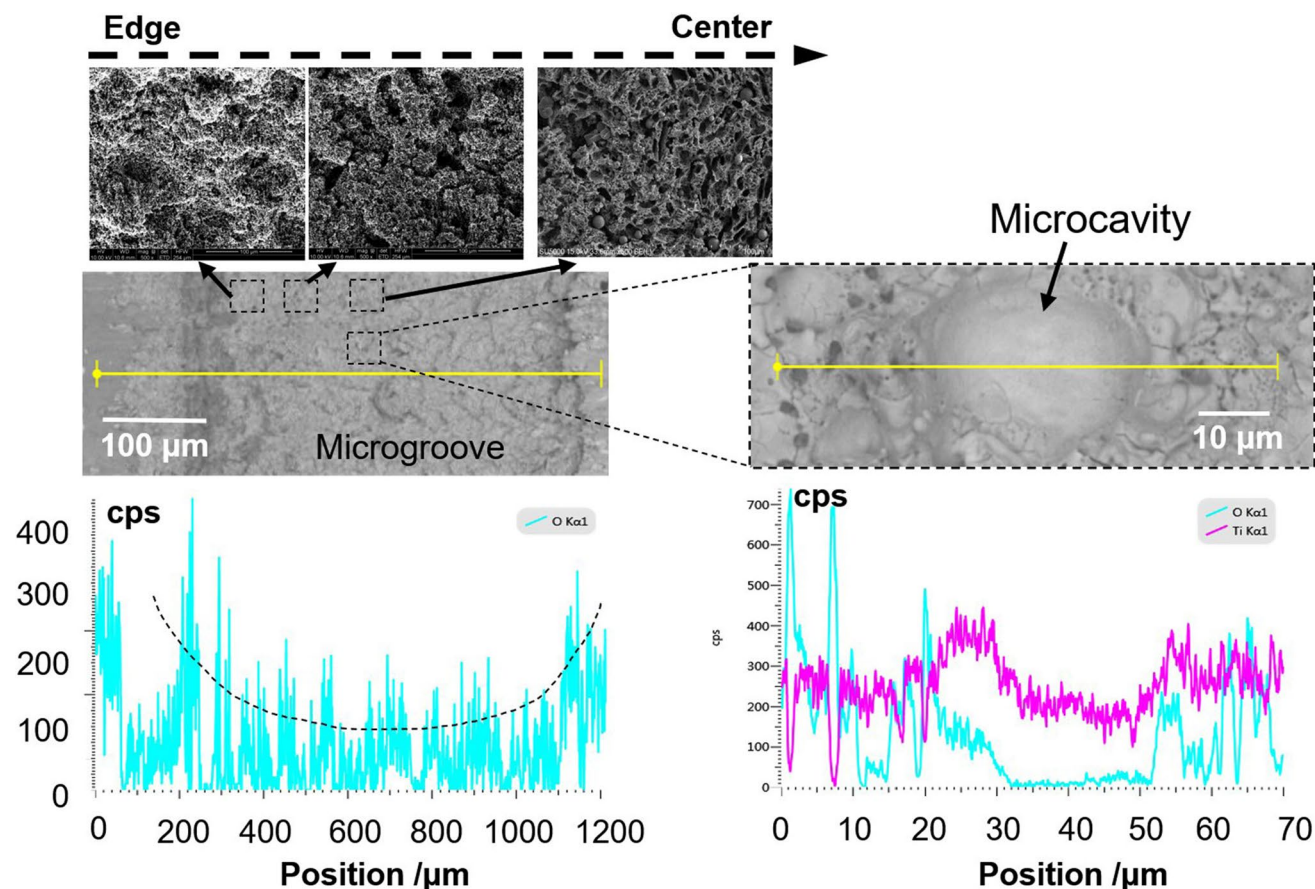


Fig. 14 SEM and EDX results for processed specimens

voltage, laser power, and electrode feeding rate on processing accuracy, MRR, surface roughness, and aspect ratio of microgrooves. The following conclusions can be drawn:

(1) Synchronous laser irradiation effectively boosts ECM's materials removal capability on titanium alloys during LECM. Laser-induced temperature elevation activates titanium alloys, enhancing electrochemical corrosion efficiency with local electrolyte temperature rise. LECM processing with 4 W laser power and 18 V voltage yielded 11.18% width increase, 441.79% depth increase, and 394.44% aspect ratio increase compared to single ECM with 18 V voltage.

(2) Optimal processing accuracy and surface roughness were achieved through LECM with 3 W laser power. At 6 W laser power, direct laser beam processing led to slot formation in the central area. Elevating laser power to 9 W resulted in deep, high-aspect-ratio slot engraving by jet-assisted laser beam, coupled with inhibited surrounding electrochemical dissolution.

(3) An equivalent electric circuit model of LECM was established, illustrating titanium alloy removal mechanisms during the process. Measurement verified the Gaussian

distribution of laser power density in the front gap. Microtopography and element distribution within processed structures were detected. The synergy between laser irradiation and electrochemical dissolution was demonstrated, clarifying the mechanism of LECM for titanium alloy materials removal.

(4) A strategy involving gradient laser power in LECM was proposed for efficient fabrication of large aspect-ratio structures. High-aspect-ratio microgrooves with flat bottoms and high precision were achieved on titanium alloys using this approach.

Author contribution YW contributed to the conception of the study, and guided experiments and conclusions; YY and CS performed the experiment, analyzed the data, and completed the manuscript; QW and JY assisted to the fabrication of experimental setup; YL, JY, and WZ funded the study.

Funding This research was supported by the Zhejiang Provincial Natural Science Foundation of China [grant number LD22E050013] and the key Research and Development Plan of Ningbo [grant number 2023Z028].

Data availability The datasets used or analyzed during the current study are available from the corresponding author on reasonable request.

Code availability Not applicable.

Declarations

Ethics approval Not applicable.

Consent to participate This study involved no ethical issues.

Consent for publication This study involved no ethical issues.

Conflict of interest The authors declare no competing interests.

References

- Quintero D, Galvis O, Calderón JA, Castaño JG, Echeverría F (2014) Effect of electrochemical parameters on the formation of anodic films on commercially pure titanium by plasma electrolytic oxidation. *Surf Coat Technol* 58:1223–1231. <https://doi.org/10.1016/j.surfcoat.2014.06.058>
- Li S, Mi G, Wang C (2020) A study on laser beam oscillating welding characteristics for the 5083 aluminum alloy: morphology, microstructure and mechanical properties. *J Manuf Process* 53:12–20. <https://doi.org/10.1016/j.jmapro.2020.01.018>
- AlShaer AW, Li L, Mistry A (2014) The effects of short pulse laser surface cleaning on porosity formation and reduction in laser welding of aluminium alloy for automotive component manufacture. *Opt Laser Technol* 64:162–171. <https://doi.org/10.1016/j.optlastec.2014.05.010>
- Ali H, Ghadbeigi H, Mumtaz K (2018) Effect of scanning strategies on residual stress and mechanical properties of selective laser melted Ti6Al4V. *Mater Sci Eng A* 712:175–187. <https://doi.org/10.1016/j.msea.2017.11.103>
- He H, Wang C, Zhang X, Ning X, Sun L (2020) Facile fabrication of multi-scale microgroove textures on Ti-based surface by coupling the re-solidification bulges derived from nanosecond laser irradiation. *Surf Coat Technol* 386:125460. <https://doi.org/10.1016/j.surfcoat.2020.125460>
- Nascimento R, Moura CG, Carvalho O, Gonçalves LMV, Cerqueira MF, Silva F (2019) Laser surface texturing of Ti-6Al-4V by nanosecond laser: surface characterization, Ti-oxide layer analysis and its electrical insulation performance. *Mater Sci Eng C Mater Biol Appl* 104:109901. <https://doi.org/10.1016/j.msec.2019.109901>
- Bloyce A, Qi PY, Dong H, Bell T (1998) Surface modification of titanium alloys for combined improvements in corrosion and wear resistance. *Surf Coat Technol* 107:125–132. [https://doi.org/10.1016/S0257-8972\(98\)00580-5](https://doi.org/10.1016/S0257-8972(98)00580-5)
- Kumar A, Gupta MC (2009) Surface preparation of Ti-3Al-2.5 V alloy tubes for welding using a fiber laser. *Opt Laser Technol* 47:1259–1265. <https://doi.org/10.1016/j.optlaseng.2009.05.011>
- Ayesta I, Izquierdo B, Sánchez JA, Ramos JM, Plaza S, Pombo I, Ortega N, Bravoe H, Fradejase R, Zamakonae I (2013) Influence of EDM parameters on slot machining in C1023 aeronautical alloy. *Procedia CIRP* 6:129–134. <https://doi.org/10.1016/j.procir.2013.03.059>
- Flaño O, Ayesta I, Izquierdo B, Sánchez JA, Zhao Y, Kunieda M (2018) Improvement of EDM performance in high-aspect ratio slot machining using multi-holed electrodes. *Precis Eng* 51:223–231. <https://doi.org/10.1016/j.precisioneng.2017.08.014>
- Gu L, Li L, Zhao W, Rajurkar KP (2012) Electrical discharge machining of Ti6Al4V with a bundled electrode. *Int J Mach Tool Manu* 53:100–106. <https://doi.org/10.1016/j.ijmactools.2011.10.002>
- Valaki JB, Rathod PP (2016) Assessment of operational feasibility of waste vegetable oil based bio-dielectric fluid for sustainable electric discharge machining (EDM). *Int J Adv Manuf Technol* 87:1509–1518. <https://doi.org/10.1007/s00170-015-7169-0>
- Raja K, Ravikumar R (2016) A review on electrochemical machining processes. *Int J Energy Res* 11:2354–2355
- Zhao J, Lv Y, Wang F, Yang Z, Liu D, Fan Y, He Y (2018) Experimental research on process stability in pulsed electrochemical machining of deep narrow grooves with high length-width ratio. *Int J Adv Manuf Technol* 96:2245–2256. <https://doi.org/10.1007/s00170-018-1610-0>
- Wang GQ, Zhu D, Li HS (2018) Fabrication of semi-circular micro-groove on titanium alloy surface by through-mask electrochemical micromachining. *J Mater Process Technol* 258:22–28. <https://doi.org/10.1016/j.jmatprotec.2018.03.015>
- Zhang C, Yao J, Zhang C, Chen X, Liu J, Zhang Y (2020) Electrochemical milling of narrow grooves with high aspect ratio using a tube electrode. *J Mater Process Technol* 282:116695. <https://doi.org/10.1016/j.jmatprotec.2020.116695>
- He Y, Xiao H, Gan W, Yu Q, Yin F (2018) The electrochemical dissolution behavior research of titanium alloy under different electrolyte. *Procedia CIRP* 68:751–756. <https://doi.org/10.1016/j.procir.2017.12.132>
- Weinmann M, Stolpe M, Weber O, Busch R, Natter H (2015) Electrochemical dissolution behaviour of Ti90Al6V4 and Ti60Al40 used for ECM applications. *J Solid State Electrochem* 19:485–495. <https://doi.org/10.1007/s10008-014-2621-x>
- Fushimi K, Habazaki H (2008) Anodic dissolution of titanium in NaCl-containing ethylene glycol. *Electrochim Acta* 53:3371–3376. <https://doi.org/10.1016/j.electacta.2007.11.074>
- Nguyen MD, Rahman M, San Wong Y (2012) Enhanced surface integrity and dimensional accuracy by simultaneous micro-ED/EC milling. *CIRP Ann* 61:191–194. <https://doi.org/10.1016/j.cirp.2012.03.011>
- Zhai K, Du L, Wen Y, Wang S, Cao Q, Zhang X, Junshan L (2020) Fabrication of micro pits based on megasonic assisted through-mask electrochemical micromachining. *Ultrasonics* 100:105990. <https://doi.org/10.1016/j.ultras.2019.105990>
- Li S, Wu Y, Nomura M, Fujii T (2018) Fundamental machining characteristics of ultrasonic-assisted electrochemical grinding of Ti-6Al-4V. *J Manuf Sci Eng* 140:071009. <https://doi.org/10.1115/1.4039855>
- Wang Y, Yang F, Zhang W (2019) Development of laser and electrochemical machining based on internal total reflection. *J Electrochem Soc* 166:E481. <https://doi.org/10.1149/2.0471914jes>
- Liu J, Bai J, Ni K, Jing H, He X, Liu D (2008) Attenuation characteristics of laser beam in water. *Acta Phys Sin* 57:1. <https://doi.org/10.7498/aps.57.260>

Publisher's note Springer Nature remains neutral with regard to jurisdictional claims in published maps and institutional affiliations.

Springer Nature or its licensor (e.g. a society or other partner) holds exclusive rights to this article under a publishing agreement with the author(s) or other rightsholder(s); author self-archiving of the accepted manuscript version of this article is solely governed by the terms of such publishing agreement and applicable law.